UiO : Department of Mathematics
University of Oslo

Monolithic solver for Computational Fluid-Structure Interaction

Sebastian Gjertsen

Master's Thesis, Spring 2017

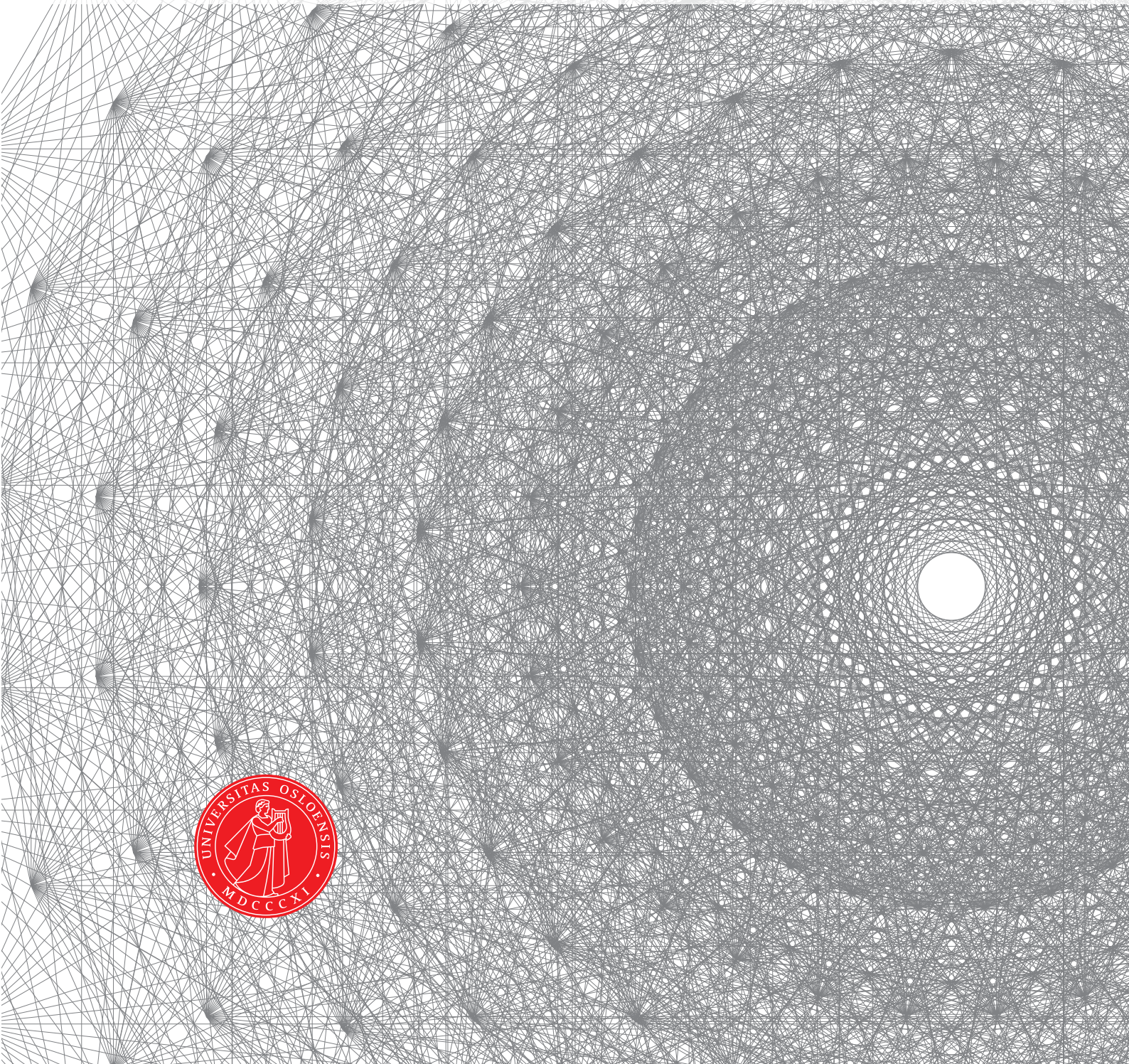

This master's thesis is submitted under the master's programme *Computational Science and Engineering*, with programme option *Mechanics*, at the Department of Mathematics, University of Oslo. The scope of the thesis is 60 credits.

The front page depicts a section of the root system of the exceptional Lie group E_8, projected into the plane. Lie groups were invented by the Norwegian mathematician Sophus Lie (1842–1899) to express symmetries in differential equations and today they play a central role in various parts of mathematics.

Contents

Chapter 1

Comparing the effects of different lifting operators and Investigating Numerical Stability in Fluid-Structure Interaction problems

The first section is devoted to comparing different lifting operators defined in section **??**. The choice of lifting operators is crucial when computing FSI problems. When handling large structural deformations one has to be very cautious about the choice of lifting operators. A good lifting operator upholds the integrity of the computational domain, allowing large deformations in the solid and into the fluid domain. The computational cost is different of the different lifting operators, and it is therefore crucial to chose the right lifting operator for a specific problem.

The second section investigates briefly the impact of choosing different value for θ in the θ-scheme. The effects of choosing a Crank-Nicholson or a backward Euler scheme is known to have effects on the energy preservation in a computational system. Also the effects of shifting the Crank-Nicholson scheme is investigated using the FSI2 and FSI3 case from the previous chapter.

1.1 Methods for comparing lifting operators

The comparisons will be performed using a version of the CSM1 test as defined the previous chapter, with the same computing domain and parameters. The version of CSM1 test case is now computed as a full FSI problem with the fluid initially at rest. A gravitational force is applied to the structure much like the previous CSM test. The only difference is that we now use the full domain from the **??**. The test is run as time-dependent with a the backward Euler scheme, leading to a steady state solution.

The tests will compare the different operators by investigating how the deformation from the solid domain is lifted into the fluid domain. I investigate plots of the mesh after deformation to see how much cells distort and where the cells distort. This is visualized using Paraview with its built in function *warp by vector*, which redistributes nodes based on the displacement values in each nodal point. The computing domain is the same as used in the Hron Turek benchmark, from the previous section. The upper, lower and left boundary is set as "no slip" condition. The left boundary is set to "do nothing", and zero pressure.

The different operators will be plotted with the minimal value of the Jacobian. The Jacobian is also known as the volume ratio, and if the Jacobian is zero anywhere in the domain it means that the volume is negative, and cells overlap. Which can cause singularity in the matrices during assembly. When cells overlap it can in the best case cause the computed numerical code to diverge, and in the worst case just give very wrong results.

A plot of the deformation in the domain has been added, to visualize how the different mesh motion techniques work. It is possible to see that if get thin triangles in the computational domain then the lifting operator is not good enough, and we might get singularities in the computing matrix. I also looked at how different lifting operators react differently in the FSI2 and FSI3 test cases from the previous section. Here I investigated plots of the lift, drag and displacements too see how the different lifting operators respond to different inflow velocities and solid parameters. Bc1 and bc2 denotes the boundary conditions 1 and 2 used when employing the biharmonic lifting operator.

Different lifting operators with testcase CSM1

Figure **??** which shows the minimum of the Jacobian of the entire domain. The harmonic operator with a constant α_u parameter, gives overlapping cells While the harmonic lifting operator with variable α_u and both the biharmonic techniques, uphold the cells quality.

Figure **??** shows the meshes of the different lifting operators, for the steady state solutions from the CSM1 test case. The harmonic with a spatial dependent variable α_u and the two biharmonic lifting operators upholds good integrity of the cells. While the harmonic lifting operator with a constant α_u shows degeneration of cells at the tip of the bar. However, the computed numerical code was able to compute with the harmonic constant α_u operator, but as we can see in table **??** the displacement values are incorrect.

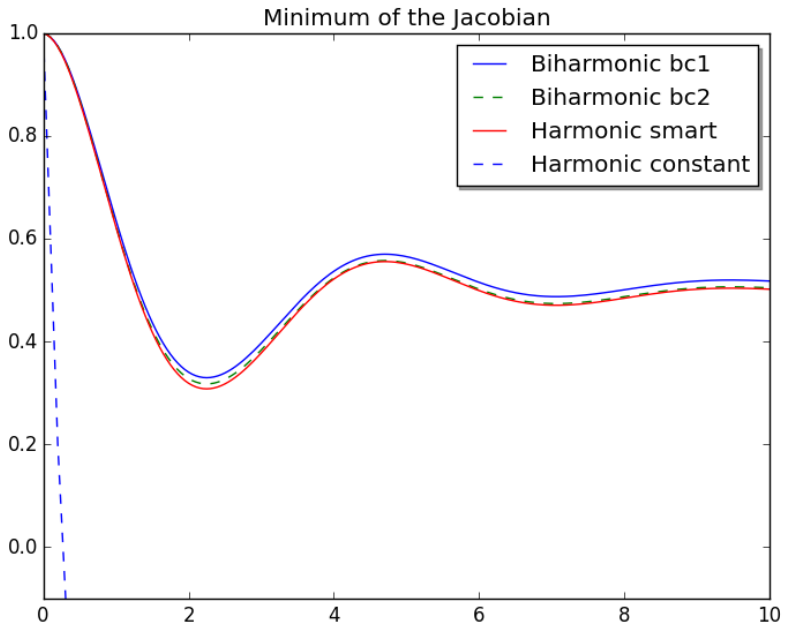

Figure 1.1: plot of the minimum of J in entire domain, using CSM1 test. $\Delta t = 0.05$

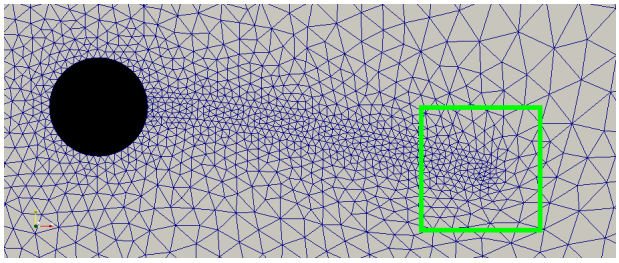

Figure 1.2: Harmonic lifting operator with spatial dependent α_u

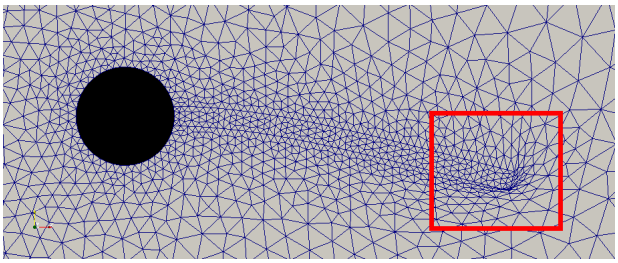

Figure 1.3: Harmonic lifting operator with constant α_u

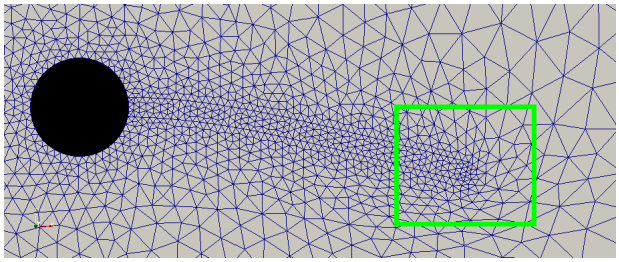

Figure 1.4: Biharmonic lifting operator with boundary condition 1

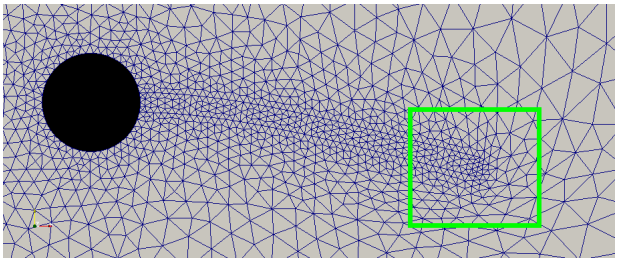

Figure 1.5: Biharmonic lifting operator with boundary conditions 2

Figure 1.6: Results of testing different lifting operator using the CSM1 test-case computing full FSI. Green square denoting good cell integrity.

Technique	$d_y(A)[\times 10^{-3}]$	$d_x(A)[\times 10^{-3}]$
Harmonic	-65.406	-7.036
Constant	-43.033	-2.999
Bibc1	-65.404	-7.036
Bibc2	-65.405	-7.036
Hron & Turek	$\mathbf{-66.10}$	$\mathbf{-7.187}$

Table 1.1: Displacements results of different lifting operators of CSM1 test

FSI2 with different Lifting operator

Figure **??** shows the harmonic and the two biharmonic mesh motion techniques for the FSI2 case. All three are similar and only a slight change in the period can be noticed.

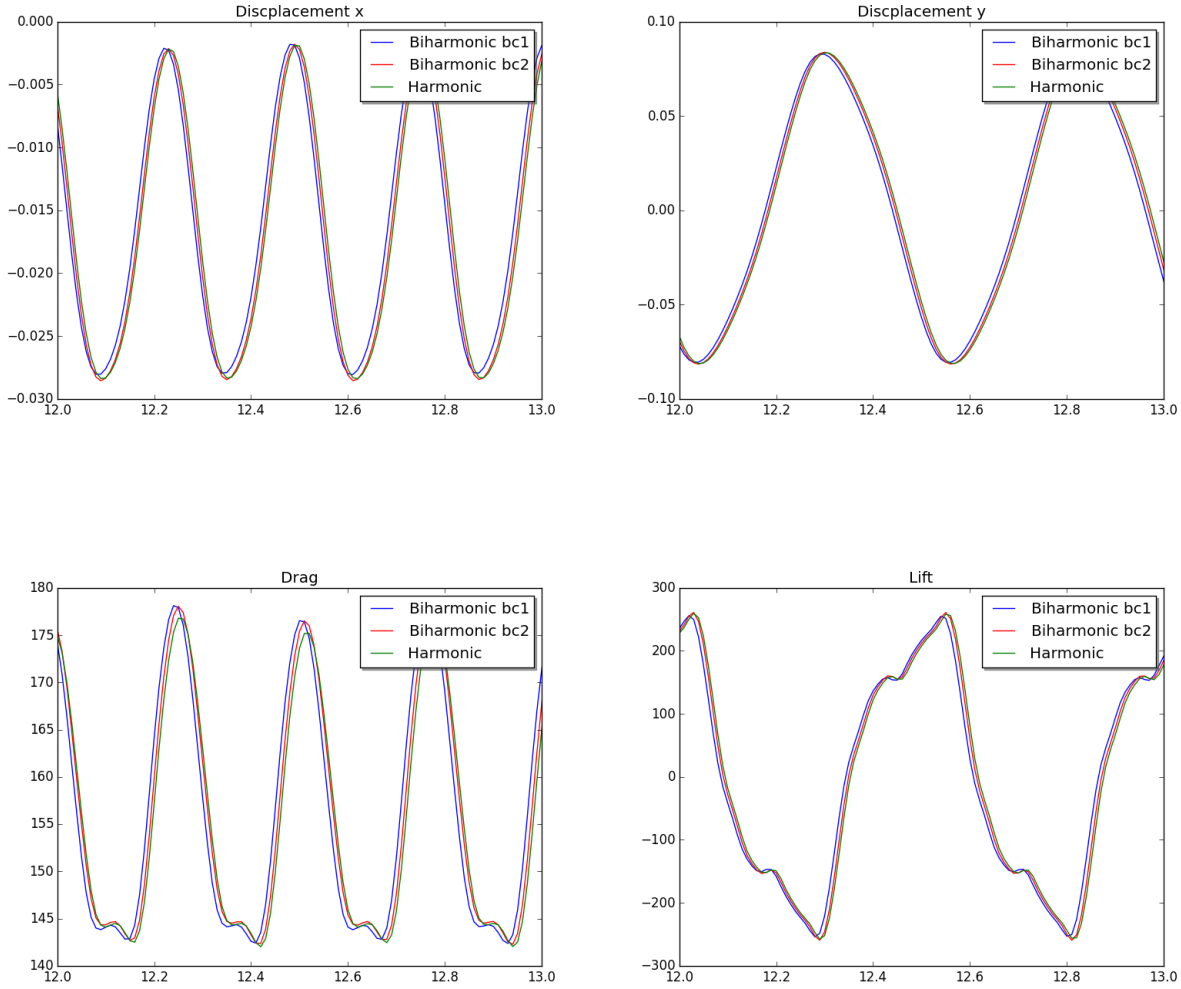

Figure 1.7: FSI2 with different lifting operators: harmonic, biharmonic bc1 and bc2. $\Delta t = 0.01$

Figure **??**, **??**, **??** and **??** shows the displacement in x and y direction, and drag and lift plots respectively. The displacements and Lift plots show only a slight change in the period. While the Drag for the harmonic lifting operator with mesh dependent α_u shows an increasing in the Drag value of about 10.

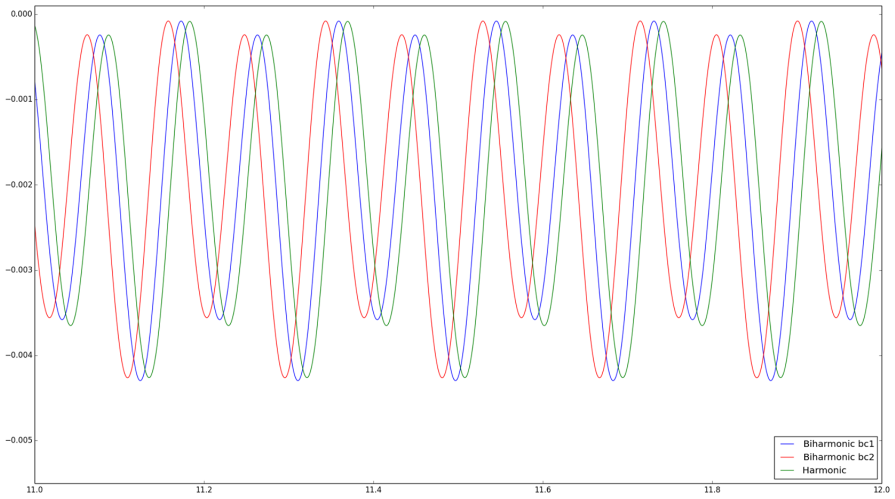

Figure 1.8: Displacement in x direction for FSI3 with different lifting operators: Harmonic, Biharmonic bc1 and bc2. $\Delta t = 0.001$

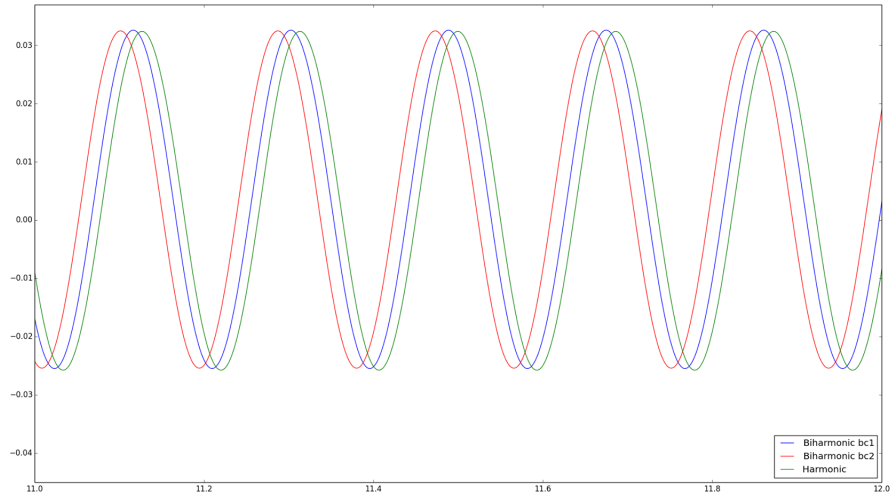

Figure 1.9: Displacement in x direction for FSI3 with different lifting operators: Harmonic, Biharmonic bc1 and bc2. $\Delta t = 0.001$

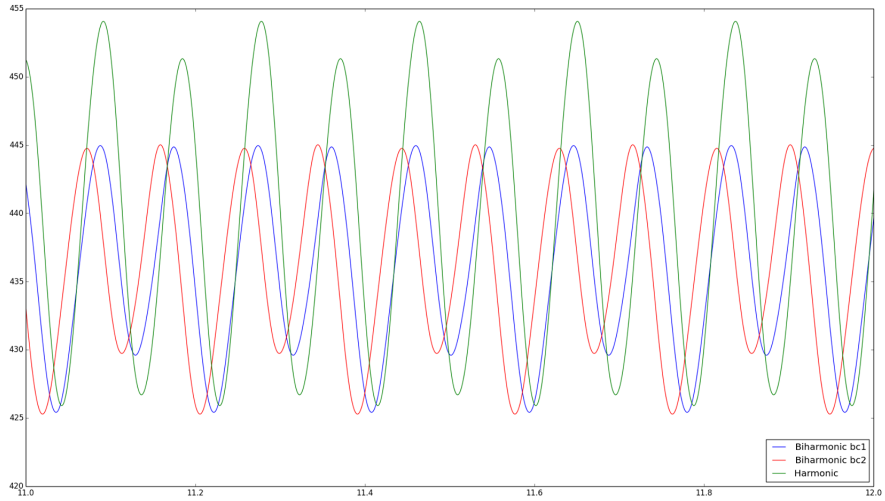

Figure 1.10: Drag results for FSI3 with different lifting operators: Harmonic, Biharmonic bc1 and bc2. $\Delta t = 0.001$

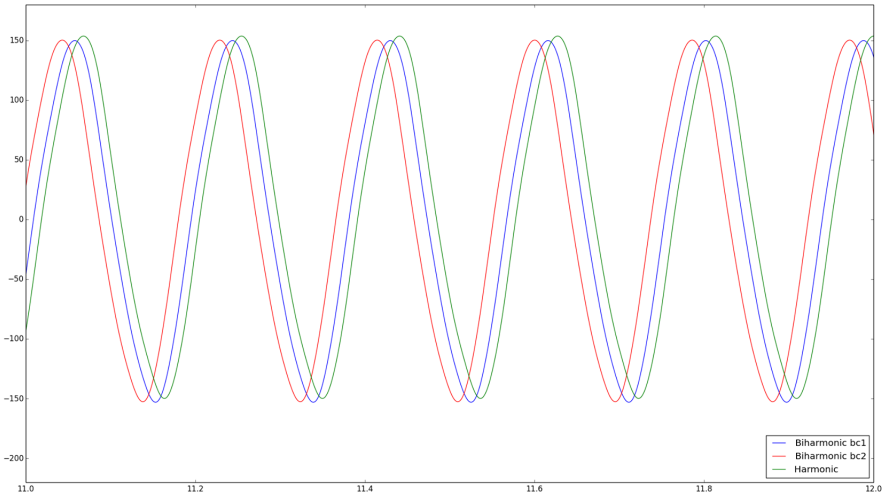

Figure 1.11: Lift results for FSI3 with different lifting operators: Harmonic, Biharmonic bc1 and bc2. $\Delta t = 0.001$

Discussion of comparing different lifting operators

In the FSI2 case all the different lifting operators show similar trend and it is seemingly not important for the results which lifting operator we use. This indicates that with a clever α_u, the harmonic technique can be chosen. This is an advantage since the harmonic techniques is the least computationally costly. Whilst when we increase the inflow speed as in the FSI3 case there is a change in the period of the unsteady solution and the drag actually gives higher values. Indicating the the biharmonic lifting operator may be a wiser choice.

In the FSI3 case there is an observed change in the drag values and the reason could be that the cells integrity are upheld in a different manner for different lifting operators. For the harmonic lifting operator it is reasonable to assume that for larger deformations the cell height on the interface will be smaller than for the biharmonic, hence giving a different value to the integrals when calculating drag. The lift and displacement differences for different lifting operators are similar. It is reasonable to assume that this is because of the normal force applied to the upper and lower sides of the bar, which is originally an effect of asymmetry in the y-direction of the domain, is what induces motion. The displacements are a secondary effect of the instability of the fluid and hence the effects we see in the values of lift are also seen in the displacements.

In short the lifting of the deformations into the fluid domain gives different cell structures which in turn effects the integral of the stress tensors on the interface. This in turns produces different results for problems with larger mesh deformations combined with high fluid velocities. This gives the conclusion that lifting operators are highly problem specific and for cases with large deformations lifting operators should be chosen with care.

It should also be noted that the biharmonic lifting operators are able to compute in parallel with multiple computer cores, while the harmonic with variable α_u is not able to run in parallel. This concludes that even though the harmonic lifting operator is is less computationally costly, computing on multiple cores is faster with the biharmonic lifting operator.

1.2 Investigating Numerical stability for Fluid-Structure Interaction Problems

The following section will give a brief insight in to the effects of choosing different θ values in the $\theta-$scheme for different time steps. The benchmark tests FSI2 and FSI3, as discussed in the previous section, has been investigated since they are known to be numerical unstable for certain values of θ and Δt. Only the effects of Drag as been studied as the three other quantities shows the same behavior.

The impact of energy stability of choosing different θ values in the solid mechanical case CSM3 is a also investigated.

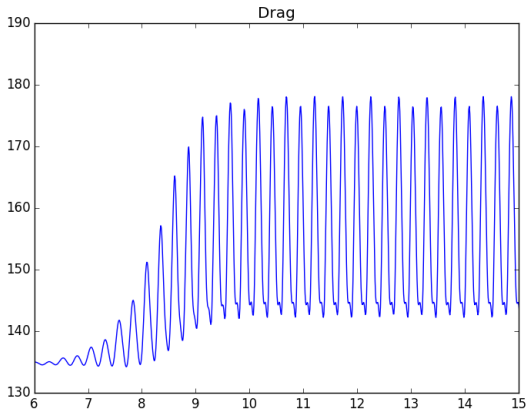

Figure 1.12: $\theta = 0.51$

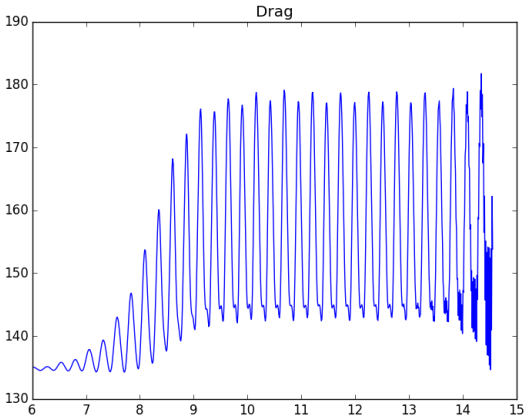

Figure 1.13: $\theta = 0.50$

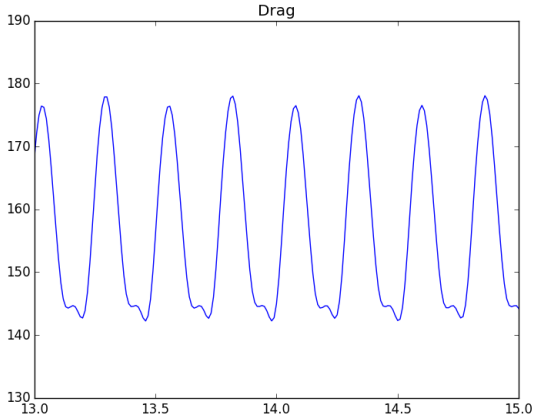

Figure 1.14: $\theta = 0.51$

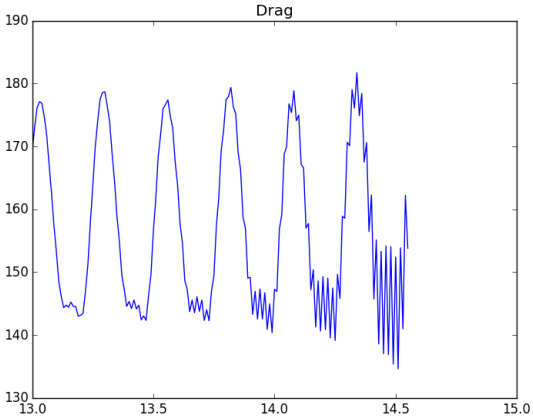

Figure 1.15: $\theta = 0.50$

Figure 1.16: Drag for FSI2 with $\Delta t = 0.01$ with different values for θ

?? show the plots of Drag with $\Delta t = 0.01$, showing the instability when choosing $\theta = 0.5$. The Crank-Nicholson scheme is stable until about 13 seconds where we see that it is numerically unstable and the solver diverges. While the shifted Crank-Nicholson, $\theta = 0.5 + \Delta t$, is stable throughout the computing time.

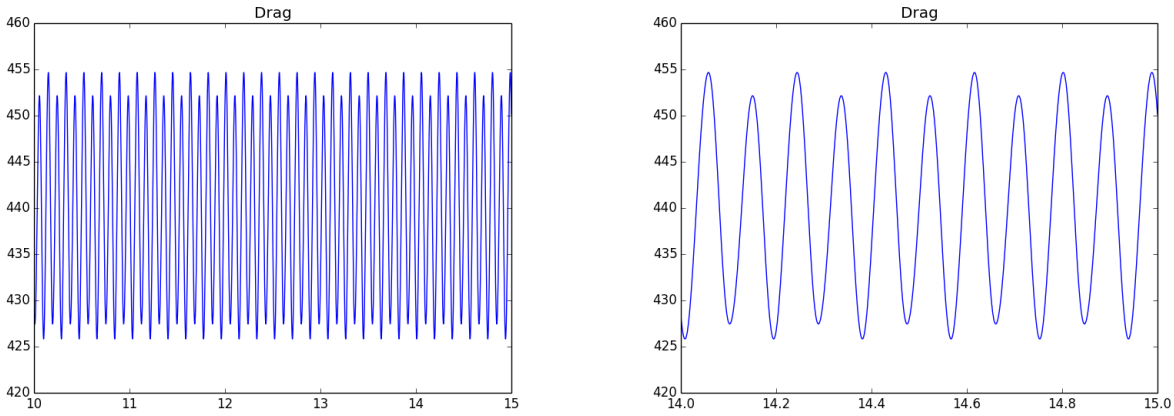

Figure 1.17: Left: Right: Disassembled bearing

Figures **??** and **??** show drag for simulation with $\Delta t = 0.001$ and $\theta = 0.5$, showing long term stability for the normal Crank-Nicholson scheme.

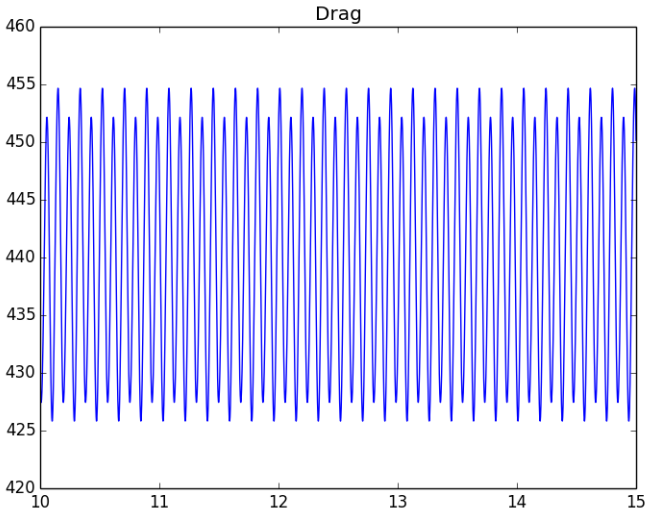

Figure 1.18: Drag for FSI3 with $\Delta t = 0.001$ with $\theta = 0.5$

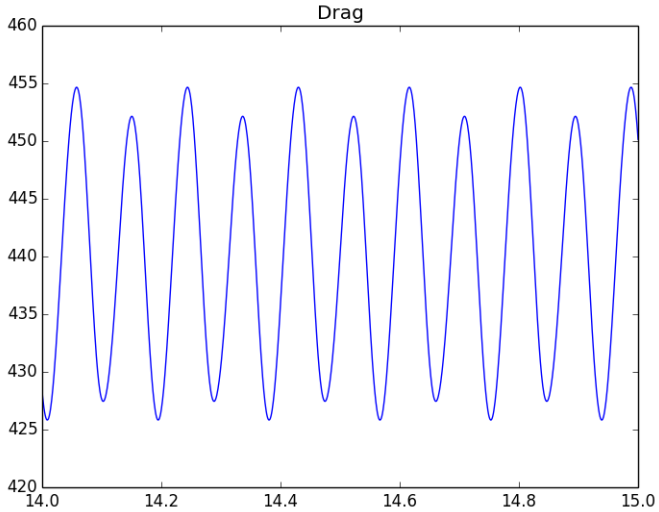

Figure 1.19: Drag for FSI3 with $\Delta t = 0.001$ with $\theta = 0.5$

Figures **??** and **??** show drag for simulation with $\Delta t = 0.001$ and $\theta = 0.5$, showing long term stability for the normal Crank-Nicholson scheme.

Figure 1.20: CSM3 displacements with $\Delta t = 0.01$ with different values for θ

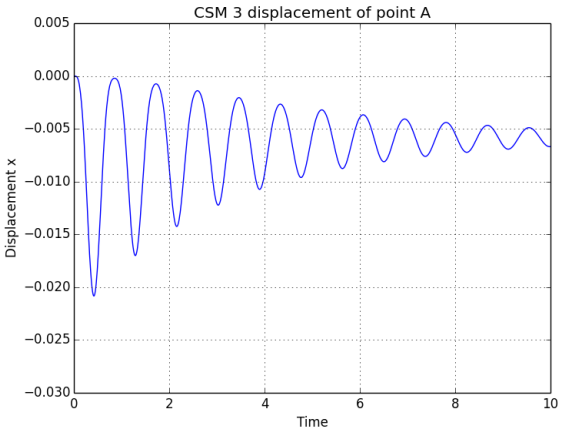

Figure 1.21: $\theta = 1$

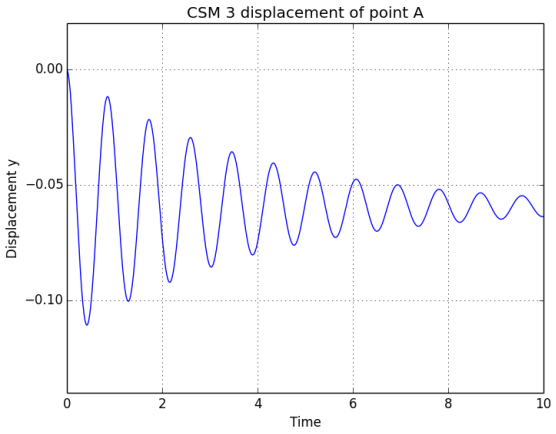

Figure 1.22: $\theta = 1$

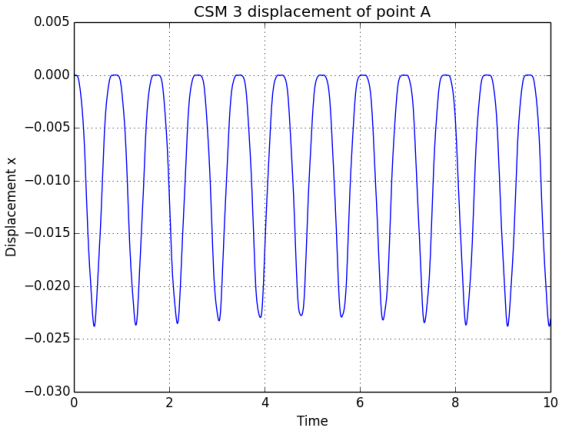

Figure 1.23: $\theta = 0.5$

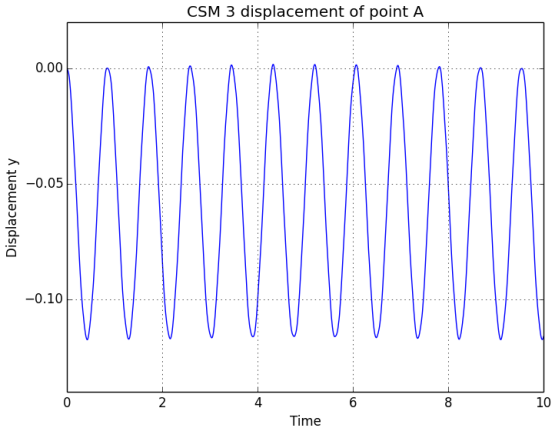

Figure 1.24: $\theta = 0.5$

Figure **??** shows plots of the displacements in x and y directions for $\theta = 0.5$ and 1. With the implicit scheme ($\theta = 1$) the bar moves to a steady state solution. This means energy has not been preserved and the energy dissipates. While in the Crank-Nicholson scheme ($\theta = 0.5$)

Discussion on numerical stability

The shifted version of the Crank-Nicholson scheme is stable when computing for time step values as low as $\Delta t = 0.01$. However with $\Delta t = 0.001$ the normal Crank-Nicholson scheme ($\theta = 0.5$) can be used and is long term stable. It has also been reported by Wick 2011 [**?**] that the Crank-Nicholson, $\theta = 0.5$, scheme is stable throughout the computing time by setting $\Delta t = 0.001$.

In the FSI2 case the results for the finest mesh showed, in previous chapter, similar results for $\Delta t = 0.01$ and $\Delta t = 0.001$, meaning that the shifted version of the Crank-Nicholson scheme can be applied, in certain cases, with $\Delta t = 0.01$ greatly reducing computational runtime.

The CSM3 test shows that choosing $\theta = 0.5$ is crucial for preserving energy when computing solid problems.

Bibliography

[1] K. Yusuf Billah. Resonance, Tacoma Narrows bridge failure, and undergraduate physics textbooks. *American Journal of Physics*, 59(2):118, 1991.

[2] David J Charlesworth. Solution of the Incompressible Navier- Stokes Equations on Unstructured Meshes by. (August), 2003.

[3] S. Étienne, A. Garon, and D. Pelletier. Some manufactured solutions for verification of fluid-structure interaction codes. *Computers and Structures*, 106-107:56–67, 2012.

[4] Stéphane Étienne, D Tremblay, and Dominique Pelletier. Code Verification and the Method of Manufactured Solutions for Fluid-Structure Interaction Problems. *36th AIAA Fluid Dynamics Conference and Exhibit*, (June):1–11, 2006.

[5] Charles L. Fefferman. Existence and smoothness of the Navier-Stokes equation. *The millennium prize problems*, (1):1–5, 2000.

[6] Miguel A. Fernández, Jimmy Mullaert, and Marina Vidrascu. Explicit robin-neumann schemes for the coupling of incompressible fluids with thin-walled structures. *Computer Methods in Applied Mechanics and Engineering*, 267:566–593, 2013.

[7] Miguel A. Fernández, Jimmy Mullaert, and Marina Vidrascu. Generalized Robin-Neumann explicit coupling schemes for incompressible fluid-structure interaction: Stability analysis and numerics. *International Journal for Numerical Methods in Engineering*, 101(3):199–229, 2015.

[8] G Holzapfel. Nonlinear solid mechanics: A continuum approach for engineering, 2000.

[9] Jaroslav Hron and Stefan Turek. Proposal for numerical benchmarking of fluid-structure interaction between an elastic object and laminar incompressible flow. *Fluid-Structure Interaction*, 53:371–385, 2006.

[10] Jie Liu, Rajeev K. Jaiman, and Pardha S. Gurugubelli. A stable second-order scheme for fluid-structure interaction with strong added-mass effects. *Journal of Computational Physics*, 270:687–710, 2014.

[11] Anders Logg, Harish Narayanan, Marie Rognes, Johannes Ring, Kristian B. Ølgaard, and Garth N. Wells. FEniCS Project, 2011.

[12] Cm Macal. Proceedings of the 2005 Winter Simulation Conference ME Kuhl, NM Steiger, FB Armstrong, and JA Joines, eds. *Simulation*, pages 1643–1649, 2005.

[13] Selim MM and Koomullil RP. Mesh Deformation Approaches – A Survey. *Journal of Physical Mathematics*, 7(2), 2016.

[14] William L. Oberkampf and Christopher J. Roy. *Verification and Validation in Scientific Computing*. Cambridge University Press, Cambridge, 2010.

[15] T Richter and T Wick. On time discretizations of Fluid-structure interactions. *Multiple Shooting and Time Domain Decomposition MEthods*, pages 377–400, 2013.

[16] Thomas Richter. Fluid Structure Interactions. 2016.

[17] Patrick J. Roache. Code Verification by the Method of Manufactured Solutions. *Journal of Fluids Engineering*, 124(1):4, 2002.

[18] M. Schäfer, S. Turek, F. Durst, E. Krause, and R. Rannacher. Benchmark Computations of Laminar Flow Around a Cylinder. pages 547–566, 1996.

[19] Natural Sciences. A Newton ' s Method Finite Element Algorithm for Fluid-Structure Interaction. (October), 2012.

[20] Noelle Selin. Verification and Validation. (February), 2014.

[21] K. Stein, T. Tezduyar, and R. Benney. Mesh Moving Techniques for Fluid-Structure Interactions With Large Displacements. *Journal of Applied Mechanics*, 70(1):58, 2003.

[22] S Turek, J Hron, M Razzaq, H Wobker, and M Sch. Fluid Structure Interaction II. 73, 2010.

[23] Boris Valkov, Chris H Rycroft, and Ken Kamrin. Eulerian method for fluid – structure interaction and submerged solid – solid contact problems.

[24] E. H. van Brummelen. Added Mass Effects of Compressible and Incompressible Flows in Fluid-Structure Interaction. *Journal of Applied Mechanics*, 76(2):021206, 2009.

[25] V Vinje. Simulating Cerebrospinal Fluid Flow and Spinal Cord Movement Associated with Syringomyelia. 2016.

[26] Frank M. White. Chapter 3 - Solutions of the Newtonian viscous-flow equa- tions. *Viscous Fluid Flow*, (5), 2006.

[27] Thomas Wick. Adaptive Finite Element Simulation of Fluid-Structure Interaction with Application to Heart-Valve Dynamics. *Institute of Applied Mathematics, University of Heidelber*, page 157, 2011.

[28] Thomas Wick. Fluid-structure interactions using different mesh motion techniques. *Computers and Structures*, 89(13-14):1456–1467, 2011.